

Dynamical confirmation of a black hole in the X-ray transient Swift J1727.8–1613

D. Mata Sánchez^{1,2}, M. A. P. Torres^{1,2}, J. Casares^{1,2}, T. Muñoz-Darias^{1,2}, M. Armas Padilla^{1,2}, and I. V. Yanes-Rizo^{1,2}

¹ Instituto de Astrofísica de Canarias, E-38205 La Laguna, Tenerife, Spain
e-mail: matasanchez.astronomy@gmail.com, dmata@iac.es

² Departamento de Astrofísica, Univ. de La Laguna, E-38206 La Laguna, Tenerife, Spain

Received August 22, 2024; accepted November 12, 2024

ABSTRACT

The X-ray transient Swift J1727.8–1613 ended its 10-month discovery outburst in June of 2024, when it reached an optical brightness comparable to pre-discovery magnitudes. With the aim of performing a dynamical study, we launched an optical spectroscopy campaign with the GTC telescope. We detected the companion star and constructed its radial velocity curve, yielding a binary orbital period of $P_{\text{orb}} = 10.8038 \pm 0.0010$ h and a radial velocity semi-amplitude of $K_2 = 390 \pm 4$ km s⁻¹. This results in a mass function of $f(M_1) = 2.77 \pm 0.09 M_{\odot}$. Combined with constraints on the binary inclination, it sets a lower limit on the compact object mass of $M_1 > 3.12 \pm 0.10 M_{\odot}$, dynamically confirming the black hole nature of the accretor. A comparison of the average spectrum in the rest frame of the companion with synthetic stellar templates supports a K4V donor that is partially (74%) veiled by the accretion disc. A refined distance measurement of 3.4 ± 0.3 kpc, together with the astrometric proper motion and the systemic velocity derived from the radial velocity curve ($\gamma = 181 \pm 4$ km s⁻¹), supports a natal kick velocity of $v_{\text{kick}} = 210_{-50}^{+40}$ km s⁻¹, at the upper end of the observed distribution.

Key words. accretion, accretion discs – stars: black holes – X-rays: binaries – Stars: individual: Swift J1727.8–1613

1. Introduction

Black hole transients (BHTs) are traditionally discovered when they enter into outburst, epochs when their accretion discs become several magnitudes brighter across the electromagnetic spectrum. Early analysis of their spectral and photometric properties enables the preliminary classification of these objects as low-mass X-ray binaries (LMXBs): systems formed by a low-mass, Roche-lobe-filling companion star transferring mass onto a compact object (whether a black hole (BH) or a neutron star (NS)). Different techniques have been developed to pinpoint the nature of the accretor, but dynamical studies, which are only feasible during the fainter quiescence, set the gold standard (see e.g. Casares & Jonker 2014 for a review).

Swift J1727.8–1613 (hereafter J1727) is the latest BHT candidate to have been discovered (on August 24 2023; Lipunov et al. 2023; Page et al. 2023). Its brightness (reaching a peak outburst optical magnitude of $r \sim 12.7$; see Wang & Bellm 2023; Baglio et al. 2023; Alabarta et al. 2023) made it a target of observational campaigns at all wavelengths, which enabled the outburst evolution to be monitored. In the X-ray, J1727 followed the canonical behaviour for BH LMXBs (e.g. Done et al. 2007; Belloni et al. 2011), transitioning between hard and soft X-ray states (see e.g. Bollemeijer et al. 2023; Miller-Jones et al. 2023). A number of studies dedicated to the X-ray event were soon published (Chatterjee et al. 2024; Liu et al. 2024; Yu et al. 2024), reporting properties such as the detection of quasi-periodic oscillations (Zhu & Wang 2024) and variable X-ray polarization (Svoboda et al. 2024b; Podgorný et al. 2024b). In radio, J1727 shows the largest resolved continuous radio jet found to date (Wood et al. 2024). Optical studies have revealed transient cold winds

and enabled the identification of a pre-outburst optical counterpart, leading to early estimates of the orbital period ($P_{\text{orb}} \sim 7.6$ h) and distance to the source ($d = 2.7 \pm 0.3$ kpc; Mata Sánchez et al. 2024, MS24a hereafter).

The soft state outburst decay of J1727 continued in the X-ray until the low luminosity transition from the soft state to the hard one was reported (March 19 2024; Russell et al. 2024; Podgorný et al. 2024a; Svoboda et al. 2024a). Optical follow-up revealed a slowly dimming optical counterpart, reaching pre-outburst quiescence levels on June 1 2024 ($\rho \sim 19.6$, as is reported by the Asteroid Terrestrial-impact Last Alert System; Tonry et al. 2018; Heinze et al. 2018; Smith et al. 2020; Shingles et al. 2021), marking the end of a 10-month long outburst.

In this work, we present a time resolved spectroscopic campaign of J1727 in quiescence. We report on the detection of absorption features in the spectra consistent with a late-type star and measure its radial velocity curve. We obtain a precise determination of the orbital period and constrain the mass of the compact object. Additionally, we refine the distance and establish the peculiar velocity of the source, ultimately revealing the natal kick of the binary. In this work, uncertainties are cited at a 68% confidence level unless otherwise specified.

2. Observations

2.1. Spectroscopy

We observed J1727 just after the outburst demise (June 1), from June 4 to July 12. A total of 13 spectroscopic epochs containing 36 spectra of 900 s integration each (see Table 1) were obtained with the 10.4-m Gran Telescopio Canarias (GTC) at the Roque

Table 1. Journal of observations.

Date (dd/mm)	Phase	#	Airmass	Seeing ($''$)	r
04/06	0.31 – 0.34	2	1.41	1.1	19.21
05/06	0.67 – 0.70	2	1.55	1.3	19.42
07/06	0.09 – 0.11	2	1.48	1.6	19.45
08/06	0.30 – 0.42	6	1.46	1.3	19.43
28/06	0.73 – 0.75	2	1.42	0.7	19.60
	0.81 – 0.84	2	1.51	0.8	
29/06	0.90 – 0.92	2	1.42	1.0	19.59
30/06	0.99 – 1.01	2	1.57	1.0	19.53
	0.15 – 0.23	4	1.43	0.9	
01/07	0.50 – 0.53	2	1.59	0.9	19.75
05/07	0.25 – 0.27	2	1.42	0.9	19.61
06/07	0.58 – 0.60	2	1.59	0.9	19.60
08/07	0.79 – 0.81	2	1.44	1.4	19.58
10/07	0.46 – 0.48	2	1.63	1.3	19.77
12/07	0.78 – 0.80	2	1.44	0.9	19.62

Notes. The orbital phase is defined from the ephemerides derived in Sec 3.1. We report the number of exposures per epoch (#), the airmass, the seeing, and the r -band magnitudes, measured from acquisition images. The latter have a typical uncertainty of ± 0.04 , dominated by the calibration of the companion star.

de los Muchachos Observatory (La Palma, Spain), equipped with the Optical System for Imaging and low-Intermediate-Resolution Integrated Spectroscopy (OSIRIS, Cepa et al. 2000). We employed a $0.8''$ slit width, 2×2 binning, and grism R2500R, resulting in a wavelength coverage of $5560\text{--}7670 \text{ \AA}$. We reduced the dataset using PYRAF and MOLLY tasks, correcting from bias, flats, calibrating in wavelength with arc lamps, and optimally extracting the spectra. We found sub-pixel drifts on the position of the [O I]-6300 sky emission line, which were employed to correct for flexure effects on the wavelength calibration. We corrected the spectra from the Earth movement using MOLLY tasks, which sets all derived velocities in this work in the heliocentric reference frame. We measured the seeing from the spatial profile of the bidimensional spectra, performing a simultaneous Gaussian fit to the target and a near field star placed in the slit ($2.7''$ to the north-east; see Fig. 4 in M24a). We limited the calculation to the spectral range of interest ($5900\text{--}6500 \text{ \AA}$), allowing us to conclude that our data is slit-limited (Table 1). The spectral dispersion is $1.02 \text{ \AA}/\text{pix}$, while the average spectral resolution is measured from arc lines to be $R = \lambda/\Delta\lambda = 2900$. We normalised the spectra through a fit to the continuum using a seventh-order polynomial.

Stellar templates of spectral types F9V-K5V and solar metallicity ($\pm 0.1 \text{ dex}$) were observed during previous campaigns with grism R2500R, slit $0.6''$ (see Table 2). They were all reduced and normalised following the same steps as for our target. Additionally, they were corrected from their observed radial velocities, as is reported in Gaia Collaboration et al. (2023), setting them all in a null-velocity frame. Finally, a Gaussian fit to the $H\alpha$ absorption line was performed in the templates to detect and correct for any remaining flexure offset.

2.2. Photometry

We analysed the r -band acquisition images obtained prior to each set of spectra. Point spread function (PSF) photometry was performed with the DAOPHOT package (Stetson 1987) in IRAF.

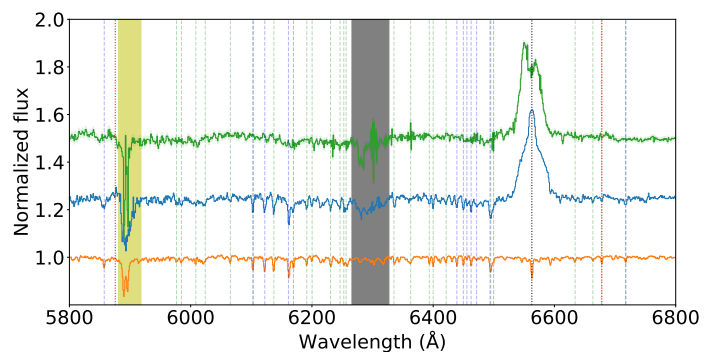


Fig. 1. Normalised, averaged spectrum of J1727 in the observer rest frame (top, solid green line), as well as in the companion star rest frame (middle, solid blue line). A template K3/4V star (HD219134) is shown in orange after applying the veiling factor derived in this work ($X_{\text{veil}} = 0.74$). They are offset vertically by 0.25 for visualisation purposes. Absorption features identified with known atomic transitions in this wavelength range are marked as dashed lines in blue for Ca I, and green for Fe I and Fe II. Disc emission lines are marked with dotted lines, black for H and red for He I. Telluric bands and interstellar absorption are marked with shaded grey and yellow regions, respectively. Note that absorption features associated with the companion star are revealed as narrow features only in the companion rest frame.

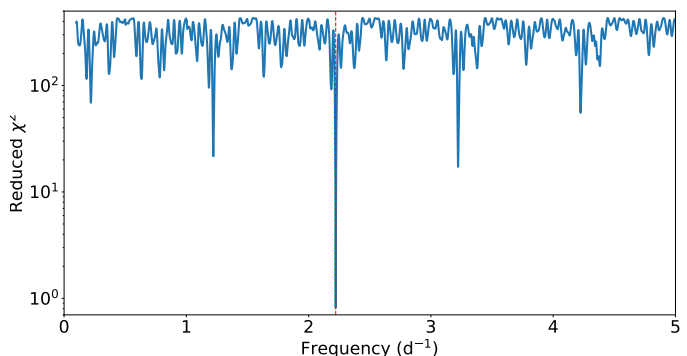


Fig. 2. Reduced χ^2 periodogram of the radial-velocity curve generated from the cross-correlation with HD 219134 (K3/4V). The best-fitting period is marked with a dashed red line. Note the logarithmic scale in the y axis.

A Moffat distribution model was constructed for five selected field stars after removing their neighbours. We performed differential photometry on the target relative to a comparison star (PSO J261.9304-16.2053, $r = 19.38 \pm 0.01$; as reported in Pan-STARRS1 Survey, Chambers et al. 2016). The resulting photometry is shown in Table 1, and yields a mean magnitude and root-mean-square variability of $r = 19.55 \pm 0.14$ for J1727 during our observations.

3. Analysis and results

The defining feature of the spectra is a double-peaked, asymmetric $H\alpha$ emission line. No other remarkable features are seen in the normalised averaged spectrum in the observer's rest frame (see Fig. 1). In what follows, we shall analyse the individual and averaged spectra in the rest frame of the companion star.

3.1. Radial velocity curve

We searched for the companion star via cross-correlation of the J1727 individual spectra with the K3/4 V template HD219134 in

Table 2. Radial velocity curve parameters (uncertainties at 1σ).

Template	T_{eff} (K)	SpecType	K_2 (km s^{-1})	γ (km s^{-1})	t_0 (d)	P_{orb} (d)	χ_{red}^2
HD 19373	5991	F9/G0 V	389 ± 4	-185 ± 3	-0.4684 ± 0.0020	0.45016 ± 0.00003	0.97
HD 186408	5815	G2 V	390 ± 4	-180 ± 3	-0.4688 ± 0.0021	0.45016 ± 0.00004	1.00
HD 186427	5762	G2 V	388 ± 4	-182 ± 3	-0.4682 ± 0.0023	0.45016 ± 0.00004	1.06
HD 235299	5471	G8 V	392 ± 4	-184 ± 3	-0.4696 ± 0.0021	0.45018 ± 0.00004	1.08
HD 185144	5260	K0 V	390 ± 4	-184 ± 3	-0.4694 ± 0.0020	0.45018 ± 0.00003	1.12
HD 219134	4717	K3/4 V	390 ± 3	-179 ± 3	-0.4681 ± 0.0019	0.45015 ± 0.00003	0.89
HD 36003	4465	K5 V	390 ± 3	-176 ± 3	-0.4685 ± 0.0020	0.45016 ± 0.00003	0.98

Notes. For the template stars we adopt the T_{eff} reported in MILES spectral library (Sánchez-Blázquez et al. 2006), except for HD 235299 (Soubiran et al. 2016). The spectral type is derived from this T_{eff} and tabulated values in Pecaut & Mamajek (2013). The best fitting parameters for the sinusoidal function described in Sect. 3.1 are also reported, being $t_0 = T_0(\text{HJD}) - 2460465.0$, and defining $\chi_{\text{red}}^2 = \chi^2/(32 \text{ d.o.f.})$.

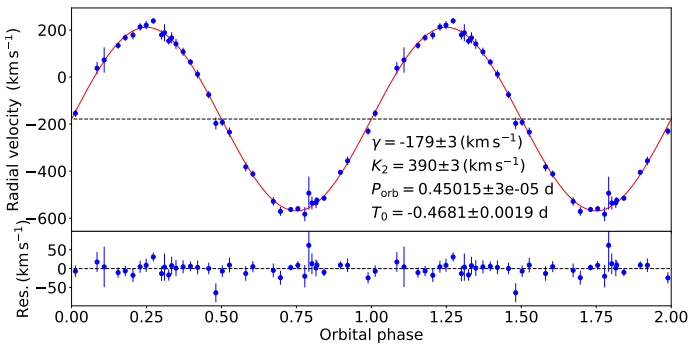


Fig. 3. Radial velocity curve of the companion star in J1727 measured through cross-correlation with the template star HD219134 (K3/4V), and folded to the best-fit ephemerides. We repeated two orbital phases for visualisation purposes. The top panel shows the individual radial velocities (blue dots), as well as the best fit sinusoid (solid red line). The best-fitting parameters are also reported in this panel. The bottom panel shows the residuals from the best fit.

the wavelength range 5920 – 6820 Å (masking out both the telluric band at 6300 Å and H α). We derived the cross-correlation functions (CCFs) using the `CROSS-CORRV` PYTHON routine from PYASTRONOMY¹. The CCFs peaks were fitted with a single Gaussian model to determine their centroids, while uncertainties on the measured radial velocities were estimated through a Monte Carlo analysis, as is described in Mata Sánchez et al. (2021). This yielded the radial velocity curve of the companion star.

We searched for periodicities in the radial velocity dataset using a χ^2 periodogram, inspecting the frequency range of $0.1 - 5 \text{ d}^{-1}$ in 10^{-5} d^{-1} frequency steps (Fig. 2). We identify a prominent peak at $\sim 0.45 \text{ d}$. The secondary peaks correspond to aliases arising from a combination of the daily repetition of the observing window with the observing cadence of $\sim 15 \text{ min}$. Indeed, attempting to perform a sinusoidal fit with a starting period value from any of the secondary peaks leads to poorly constrained fits ($\chi_{\text{red}}^2 > 20$). Only the strongest peak produces a radial velocity curve with a sinusoidal pattern, which we model as:

$$v(t) = \gamma + K_2 \sin((t - T_0)/P_{\text{orb}}),$$

where P_{orb} is the binary orbital period, K_2 the radial velocity semi-amplitude of the companion star, γ the systemic velocity, t the observation heliocentric Julian date (HJD), and $T_0(\text{HJD})$ the reference time at the inferior conjunction of the companion.

¹ <https://github.com/sczesla/PyAstronomy>

Figure 3 shows the radial velocity curve folded on the obtained ephemeris.

We repeated the above process to compare J1727 with each template of Table 2, covering spectral types F9V to K5V. The best-fitting parameters obtained are fully consistent within uncertainties, HD 219134 (K3/4V) being the best-fitting template. The largest spread is shown by γ (still consistent within 1.5σ), which we associate with uncertainties in the correction of their radial velocities. Adding the normal distributions for the parameters obtained for each template (see Table 2) leads to the following 1σ solution:

$$\begin{aligned} \gamma &= 181 \pm 4 \text{ km s}^{-1} & K_2 &= 390 \pm 4 \text{ km s}^{-1} \\ P_{\text{orb}} &= 0.45016 \pm 0.00004 \text{ d} \\ T_0(\text{HJD}) &= 2460464.5313 \pm 0.0021 \text{ d}. \end{aligned}$$

3.2. Companion star spectral type

The orbital solution allows us to correct the individual spectra from the orbital motion, and produce an average normalised spectrum in the companion rest frame (Fig. 1, middle spectrum). We employed it for its spectral type classification, considering the same wavelength range as for the cross-correlation and following the approach described in Mata Sánchez et al. (2021), based on the EMCEE Markov chain Monte Carlo sampler (Foreman-Mackey et al. 2013). This method consists of comparing the average spectra in the companion rest frame with a synthetic grid of templates constructed from the sample in Coelho (2014). The templates were degraded to the instrumental resolution of our observations ($R = 2900$), and we restricted our analysis to solar metallicity models. The synthetic templates are defined by the following parameters: the effective temperature (T_{eff}), surface gravity ($\log g$), rotational broadening ($v_{\text{sin } i}$), and velocity shift (v_{shift}) to account for potential offsets given the dispersion in γ with the spectral type of Table 2), and veiling factor (X_{veil}), defined as the ratio of fluxes of non-stellar origin to the total emitted light at the observed range of wavelengths (covering the r band).

We set the same uniform priors on the parameters as are described in Mata Sánchez et al. (2021). These put loose but physical constraints on the parameter space, and result in the corner plot in Fig. A.1. We report the 16, 50, and 84% confidence levels of the marginalised distributions for the inspected parameters (corresponding to 1σ uncertainties on a Gaussian distribution). For those parameters for which only a lower or upper limit is provided, we report the 16 or 84% confidence levels, respectively:

$$T_{\text{eff}} = 4570_{-100}^{+90} \text{ K} \quad X_{\text{veil}} = 0.74 \pm 0.02$$

$$v_{\text{sin } i} < 52 \text{ km s}^{-1} \quad v_{\text{shift}} = -4 \pm 4 \text{ km s}^{-1} \quad \log g > 4.45.$$

T_{eff} is well constrained and corresponds to a spectral type of $K4 \pm 1$ V for the companion star (Pecaut & Mamajek 2013), in line with the best-fitting template used in the cross-correlation analysis. The relatively high veiling factor (X_{veil}) implies a large contribution from the accretion disc. In this regard, the optical counterpart was 0.4 magnitudes brighter than in the pre-outburst imaging (MS24a). We cannot confidently measure the rotational broadening, which suggests a relatively low value (e.g. comparable or lower than our spectral resolution). The analysis also favours a lower limit of $\log g$ typical of dwarf stars. Finally, the v_{shift} is consistent with zero, indicating that γ was properly determined in the previous section.

4. Discussion

The analysis of the J1727 spectra during early quiescence enabled the measurement of key parameters of the system, which are discussed below.

4.1. From P_{orb} to the black hole mass

We directly measured $P_{\text{orb}} = 10.8038 \pm 0.0010$ h, longer than the value predicted in MS24a ($P_{\text{orb}} \sim 7.6$ h), using an empirical relation between P_{orb} and the outburst optical amplitude (see Shahbaz & Kuulkers 1998; also López et al. 2019 for a discussion). Together with K_2 , it allows us to derive the mass function, which imposes a conservative lower limit on the compact object mass:

$$f(M_1) = \frac{M_1 \sin^3 i}{(1+q)^2} = \frac{K_2^3 P_{\text{orb}}}{2\pi G} = 2.77 \pm 0.09 M_{\odot}; \quad q = \frac{M_2}{M_1},$$

where M_1 and M_2 are the compact object and the companion star masses, respectively, q is the mass ratio, and i is the orbital inclination.

A conservative theoretical upper limit of $\lesssim 3 M_{\odot}$ (Kalogera & Baym 1996) is often employed to discriminate NSs from BHs. However, we find that $f(M_1) = 2.77 \pm 0.09 M_{\odot}$, which is a strict lower limit on the compact object mass assuming the limiting case of $q \sim 0$ and $i = 90$ deg. Sensible constraints on both parameters are discussed below in order to fully confirm the BH nature of the compact object.

The determination of a precise q value is traditionally achieved by measuring the rotational broadening of the companion star absorption lines (see e.g. Torres et al. 2020). However, this requires templates taken with the same instrumental set-up as the target observations, which we lack. We can set constraints on q using the spectral type derived from our analysis ($K4 \pm 1$ V). Previous studies have revealed that most LMXB companions are not main-sequence stars, but instead slightly evolved (see Rappaport & Joss 1983; Podsiadlowski et al. 2003). As a result, the mass associated with the derived spectral type is better understood as an upper limit on the true companion star mass, which for J1727 results in $M_2 < 0.78 M_{\odot}$. A direct comparison can be drawn with GRS 1124–684, a BH LMXB with a similar $P_{\text{orb}} \sim 10.4$ h (González Hernández et al. 2017), donor spectral type K3–5 V (Orosz et al. 1996; Casares et al. 1997), and $q = 0.079 \pm 0.007$ (Wu et al. 2015). A similar mass ratio in J1727 would imply $M_1 > 3.22 \pm 0.10 M_{\odot}$, above the NS threshold.

Arguably the most critical parameter to fully solve the dynamical mass of LMXBs is i . The BH nature of the accretor in J1727 is independently confirmed if $i < 74$ deg ($q \sim 0$); that is, as long as an edge-on scenario is rejected. For non-eclipsing LMXBs, direct measurement of i is traditionally done through photometric light curve modelling of the ellipsoidal modulation produced by the distorted companion star (e.g. Casares & Jonker 2014). We do not detect this periodic variability in our photometry. We rather propose that the variability of the light curve ($\sigma_r = 0.14$) is instead dominated by flickering of the accretion disc (see e.g. Zurita et al. 2003). The equivalent width of the $H\alpha$ profile across our sample varies between $EW = 10 - 21 \text{ \AA}$, with the largest values observed at the faintest epochs, as was expected from variability dominated by the accretion disc fading in brightness towards its quiescence. No modulation in the EW akin to that observed in the BHT MAXI J1820+070 (Torres et al. 2019) was found at the P_{orb} , arguing against a high-inclination configuration.

X-ray observations allow us to further explore this elusive parameter. X-ray dips, a feature observed in LMXBs with inclinations > 60 deg (Frank et al. 1987), have not been reported for J1727, despite the intense monitoring enabled by its bright outburst event. Finally, radio observations of the source revealed the largest resolved continuous jet ever discovered in a LMXB (Wood et al. 2024), and imposed an upper limit on the jet inclination of < 74 deg. Assuming that the jet is launched perpendicular to the orbital plane, it would serve as proxy for i . Setting this constraint alone implies a compact object mass of $M_1 > 3.12 \pm 0.10 M_{\odot}$, placing it above the most conservative mass threshold at 1σ . We therefore conclude that all the available evidence supports the BH nature of J1727.

4.2. The distance and the peculiar velocity of J1727

MS24a proposed a distance of 2.7 ± 0.3 kpc from a number of arguments based on both optical and X-ray observations. Except for the method that directly provides the distance based on the interstellar Ca II doublet EW ratio ($d = 3.2 \pm 0.6$ kpc), the rest rely on determining the reddening and P_{orb} , with the latter utilised to derive the absolute magnitude of the optical counterpart (M_r , Casares 2018). We updated the results from MS24a using our spectroscopic measurement of P_{orb} , which makes the system brighter ($M_r = 5.92 \pm 0.11$) and consequently increases the final estimated distance. Estimates for the colour excess of $E(B - V) = 0.9 \pm 0.3$ and 0.8 ± 0.3 were found from interstellar absorption features in the outburst optical spectra, while $E(B - V) = 0.47 \pm 0.13$ were found from modelling of X-ray data, all of which are reported in MS24a. Dust maps from the Pan-STARRS1 Survey (Green et al. 2019) reveal a moderate distance dependence, $E(B - V) = 0.23 \pm 0.04$ for $d = 1 - 4$ kpc and $E(B - V) = 0.33 \pm 0.03$ for larger distances. This is lower than any of the results from the aforementioned dedicated methods, which suggests that the extinction towards J1727 is dominated by an unresolved interstellar structure in the dust maps. Taking into account these estimates for the colour excess, we updated the distance towards J1727 to $d = 2.6 \pm 0.9$ kpc, 2.9 ± 1.0 kpc, and 4.0 ± 0.6 kpc, respectively. Moreover, we can use the results from Sect. 3 to calculate the spectroscopic distance assuming a dwarf companion of spectral type K4V. Tabulated absolute magnitudes exist (Pecaut & Mamajek 2013), which we transformed following Jordi et al. (2006) to obtain an absolute magnitude in the r-band of 6.6 ± 0.5 . To properly derive the distance from this value, we need the companion star apparent magnitude. This is

$r = 21.13 \pm 0.05$, obtained from the observed magnitude in our acquisition images ($r = 19.55 \pm 0.14$) and the veiling factor derived from the spectroscopy ($X_{\text{veil}} = 0.74 \pm 0.02$). Correcting from reddening with the same set of colour excess estimates introduced above, it results in $d = 3.2 \pm 1.3$ kpc, 3.5 ± 1.5 kpc, and 4.8 ± 1.4 kpc, respectively.

The spread in the resulting d from each of the above methods highlights how complicated it is to measure a precise distance in the absence of parallax. Assuming all of the aforementioned methods are equally reliable, we calculated the conditional probability through the multiplication of the individual distributions. We obtained a final distance, fully coincident with the weighted average and weighted standard deviation, of $d = 3.4 \pm 0.3$ kpc (i.e. $|z| = 0.61 \pm 0.06$ kpc below the Galactic plane). We employed this result hereafter in our calculations; it corresponds to a range of $d = 2.5 - 4.3$ kpc at the 3σ confidence level. Using our favoured d , the soft-to-hard state transition ($\sim 0.1 - 1.2$ cts s^{-1} , Podgorný et al. 2024b) occurs at $0.01 - 0.02 L_{\text{Edd}}$ (L_{Edd} being the Eddington luminosity of a canonical BH)², within the expected range (see Maccarone 2003; Dunn et al. 2010).

An astrometric solution for the optical counterpart to J1727 is reported in *Gaia* Data Release 3 (Gaia Collaboration et al. 2016, 2023). While the proposed parallax is not particularly constraining, there is a proper motion reported for the system of $\Delta\alpha = -0.04 \pm 0.60$ mas yr^{-1} and $\Delta\delta = -4.92 \pm 0.43$ mas yr^{-1} . Combined with the distance ($d = 3.4 \pm 0.3$ kpc) and systemic velocity ($\gamma = 181 \pm 4$ km s^{-1}) measured in the present work, we derived the space velocity in the local standard of rest (U, V, W) = $(-148 \pm 5, -88 \pm 10, -71 \pm 10)$ km s^{-1} . The latter is based on Johnson & Soderblom (1987) transformations and assumes a solar space velocity in the same rest frame of $(U_{\odot}, V_{\odot}, W_{\odot}) = (9, 12, 7)$ km s^{-1} (Mihalas & Binney 1981), resulting in a space velocity of $v_{\text{space}} = 194 \pm 5$ km s^{-1} for J1727. We note that the dominant contribution to v_{space} and its uncertainty is the radial velocity component (γ). We can transform this result to a peculiar velocity referred to the J1727 Galactic neighbourhood, assuming the galactocentric potential MW-POTENTIAL2014 from the GALPY package (Bovy 2015), obtaining $(U_{\text{pec}}, V_{\text{pec}}, W_{\text{pec}}) = (-174 \pm 4, -75 \pm 10, -66 \pm 10)$ km s^{-1} . The large resulting $v_{\text{pec}} = 201 \pm 7$ km s^{-1} suggests that a kick was imparted to the system at birth. Following Atri et al. (2019)³ to integrate the Galactocentric orbit 10 Gyr back in time, we obtain a distribution of potential natal kick velocities, with 5, 50, and 95% percentiles of $v_{\text{kick}} = 210^{+40}_{-50}$ km s^{-1} . This is consistent with the upper end of natal kicks for the BH population presented in the aforementioned work, and further supports supernova models over direct collapse for the birth of the BH in J1727.

5. Conclusions

We present a spectroscopic study of the recently discovered BHT candidate J1727 in early quiescence. Phase-resolved spectroscopy reveals stellar features from a veiled ($X_{\text{veil}} = 0.74 \pm 0.02$) K4V ($T_{\text{eff}} = 4570^{+90}_{-100}$ K) companion star, which allows us to perform a dynamical study. We measure $P_{\text{orb}} = 0.45016 \pm$

² We calculate L_{Edd} for a prototypical BH ($M_1 = 8 M_{\odot}$), and convert it to flux units using $d = 3.4 \pm 0.3$ kpc. We also apply a bolometric correction of 2.9 (with 25% uncertainty, see in't Zand et al. 2007), and finally convert to cts s^{-1} for the MAXI GSC instrument in the 2-20 keV band using the WebPIMMS tool [https://heasarc.gsfc.nasa.gov/cgi-bin/Tools/w3pimms/w3pimms.pl].

³ We employed the public script available at the github link https://github.com/pikkyatri/BHnatalkicks.

0.00004 d and $K_2 = 390 \pm 4$ km s^{-1} , which results in a mass function of $f(M_1) = 2.77 \pm 0.09 M_{\odot}$. We present arguments against a fully edge-on system geometry, which allow us to set a robust lower limit on the compact object mass of $M_1 > 3.12 \pm 0.10 M_{\odot}$, confirming the BH nature of the compact object. We further refine the distance to the system with our updated binary parameters to be 3.4 ± 0.3 kpc. Combined with the systemic velocity and previous reports on the proper motion, we obtain a natal kick for the BH of $v_{\text{kick}} = 210^{+40}_{-50}$ km s^{-1} (at 5, 50, and 95% percentiles).

Acknowledgements. DMS, MAPT and TMD acknowledge support by the Spanish Ministry of Science via the Plan de Generacion de conocimiento PID2021-124879NB-I00, and JC via PID2022-143331NB-I00. MAP acknowledges support through the Ramón y Cajal grant RYC2022-035388-I, funded by MCIU/AEI/10.13039/501100011033 and FSE+. We are thankful to the GTC staff for performing the observations. This work has made use of data from the European Space Agency (ESA) mission *Gaia* (https://www.cosmos.esa.int/gaia), processed by the *Gaia* Data Processing and Analysis Consortium (DPAC, https://www.cosmos.esa.int/web/gaia/dpac/consortium). Funding for the DPAC has been provided by national institutions, in particular the institutions participating in the *Gaia* Multilateral Agreement. We are deeply grateful to Tom Marsh for developing the MOLLY software, one of his many contributions to advancing the field of compact objects. PYRAF is the python implementation of IRAF maintained by the community. The Pan-STARRS1 Surveys (PS1) and the PS1 public science archive have been made possible through contributions by the Institute for Astronomy, the University of Hawaii, the Pan-STARRS Project Office, the Max-Planck Society and its participating institutes, the Max Planck Institute for Astronomy, Heidelberg and the Max Planck Institute for Extraterrestrial Physics, Garching, The Johns Hopkins University, Durham University, the University of Edinburgh, the Queen's University Belfast, the Harvard-Smithsonian Center for Astrophysics, the Las Cumbres Observatory Global Telescope Network Incorporated, the National Central University of Taiwan, the Space Telescope Science Institute, the National Aeronautics and Space Administration under Grant No. NNX08AR22G issued through the Planetary Science Division of the NASA Science Mission Directorate, the National Science Foundation Grant No. AST1238877, the University of Maryland, Eotvos Lorand University (ELTE), the Los Alamos National Laboratory, and the Gordon and Betty Moore Foundation. This work has made use of data from the Asteroid Terrestrial-impact Last Alert System (ATLAS) project. The Asteroid Terrestrial-impact Last Alert System (ATLAS) project is primarily funded to search for near earth asteroids through NASA grants NN12AR55G, 80NSSC18K0284, and 80NSSC18K1575; byproducts of the NEO search include images and catalogues from the survey area. This work was partially funded by Kepler/K2 grant J1944/80NSSC19K0112 and HST GO-15889, and STFC grants ST/T000198/1 and ST/S006109/1. The ATLAS science products have been made possible through the contributions of the University of Hawaii Institute for Astronomy, the Queen's University Belfast, the Space Telescope Science Institute, the South African Astronomical Observatory, and The Millennium Institute of Astrophysics (MAS), Chile. We thank the referee for their useful comments that helped improve the manuscript.

References

- Alabarta, K., Russell, D. M., Baglio, M. C., et al. 2023, *The Astronomer's Telegram*, 16232, 1
- Atri, P., Miller-Jones, J. C. A., Bahramian, A., et al. 2019, *MNRAS*, 489, 3116
- Baglio, M. C., Casella, P., Testa, V., et al. 2023, *The Astronomer's Telegram*, 16225, 1
- Belloni, T. M., Motta, S. E., & Muñoz-Darias, T. 2011, *Bulletin of the Astronomical Society of India*, 39, 409
- Bollemeijer, N., Uttley, P., Buisson, D., et al. 2023, *The Astronomer's Telegram*, 16247, 1
- Bovy, J. 2015, *ApJS*, 216, 29
- Casares, J. 2018, *MNRAS*, 473, 5195
- Casares, J., & Jonker, P. G. 2014, *Space Sci. Rev.*, 183, 223
- Casares, J., Martín, E. L., Charles, P. A., Molaro, P., & Rebolo, R. 1997, *New A*, 1, 299
- Cepa, J., Aguiar, M., Escalera, V. G., et al. 2000, in *Society of Photo-Optical Instrumentation Engineers (SPIE) Conference Series*, Vol. 4008, *Optical and IR Telescope Instrumentation and Detectors*, ed. M. Iye & A. F. Moorwood, 623–631
- Chambers, K. C., Magnier, E. A., Metcalfe, N., et al. 2016, *arXiv e-prints*, arXiv:1612.05560
- Chatterjee, K., Mondal, S., Singh, C. B., & Sugizaki, M. 2024, *arXiv e-prints*, accepted for publication in *ApJ*, arXiv:2405.01498

- Coelho, P. R. T. 2014, MNRAS, 440, 1027
- Done, C., Gierliński, M., & Kubota, A. 2007, A&A Rev., 15, 1
- Dunn, R. J. H., Fender, R. P., Körding, E. G., Belloni, T., & Cabanac, C. 2010, MNRAS, 403, 61
- Foreman-Mackey, D., Hogg, D. W., Lang, D., & Goodman, J. 2013, PASP, 125, 306
- Frank, J., King, A. R., & Lasota, J. P. 1987, A&A, 178, 137
- Gaia Collaboration, Prusti, T., de Bruijne, J. H. J., et al. 2016, A&A, 595, A1
- Gaia Collaboration, Vallenari, A., Brown, A. G. A., et al. 2023, A&A, 674, A1
- González Hernández, J. I., Suárez-Andrés, L., Rebolo, R., & Casares, J. 2017, MNRAS, 465, L15
- Green, G. M., Schlafly, E., Zucker, C., Speagle, J. S., & Finkbeiner, D. 2019, ApJ, 887, 93
- Heinze, A. N., Tonry, J. L., Denneau, L., et al. 2018, AJ, 156, 241
- in't Zand, J. J. M., Jonker, P. G., & Markwardt, C. B. 2007, A&A, 465, 953
- Johnson, D. R. H. & Soderblom, D. R. 1987, AJ, 93, 864
- Jordi, K., Grebel, E. K., & Ammon, K. 2006, A&A, 460, 339
- Kalogera, V. & Baym, G. 1996, ApJ, 470, L61
- Lipunov, V., Kornilov, V., Gorbovskoy, E., et al. 2023, GRB Coordinates Network, 34536, 1
- Liu, H.-X., Xu, Y.-J., Zhang, S.-N., et al. 2024, arXiv e-prints, arXiv:2406.03834
- López, K. M., Jonker, P. G., Torres, M. A. P., et al. 2019, MNRAS, 482, 2149
- Maccarone, T. J. 2003, A&A, 409, 697
- Mata Sánchez, D., Muñoz-Darias, T., Armas Padilla, M., Casares, J., & Torres, M. A. P. 2024, A&A, 682, L1
- Mata Sánchez, D., Rau, A., Álvarez Hernández, A., et al. 2021, MNRAS, 506, 581
- Mihalas, D. & Binney, J. 1981, Galactic astronomy. Structure and kinematics
- Miller-Jones, J. C. A., Bahramian, A., Altamirano, D., et al. 2023, The Astronomer's Telegram, 16271, 1
- Orosz, J. A., Bailyn, C. D., McClintock, J. E., & Remillard, R. A. 1996, ApJ, 468, 380
- Page, K. L., Dichiarà, S., Gropp, J. D., et al. 2023, GRB Coordinates Network, 34537, 1
- Pecaut, M. J. & Mamajek, E. E. 2013, ApJS, 208, 9
- Podgorný, J., Svoboda, J., & Dovciak, M. 2024a, The Astronomer's Telegram, 16541, 1
- Podgorný, J., Svoboda, J., Dovciak, M., et al. 2024b, A&A, 686, L12
- Podsiadlowski, P., Rappaport, S., & Han, Z. 2003, MNRAS, 341, 385
- Rappaport, S. A. & Joss, P. C. 1983, in Accretion-Driven Stellar X-ray Sources, ed. W. H. G. Lewin & E. P. J. van den Heuvel, 13
- Russell, T. D., Carotenuto, F., Miller-Jones, J. C. A., et al. 2024, The Astronomer's Telegram, 16552, 1
- Sánchez-Blázquez, P., Peletier, R. F., Jiménez-Vicente, J., et al. 2006, MNRAS, 371, 703
- Shahbaz, T. & Kuulkers, E. 1998, MNRAS, 295, L1
- Shingles, L., Smith, K. W., Young, D. R., et al. 2021, Transient Name Server AstroNote, 7, 1
- Smith, K. W., Smartt, S. J., Young, D. R., et al. 2020, PASP, 132, 085002
- Soubiran, C., Le Campion, J.-F., Brouillet, N., & Chemin, L. 2016, A&A, 591, A118
- Stetson, P. B. 1987, PASP, 99, 191
- Svoboda, J., Dovciak, M., Egron, E., et al. 2024a, The Astronomer's Telegram, 16596, 1
- Svoboda, J., Dovciak, M., Steiner, J. F., et al. 2024b, ApJ, 966, L35
- Tonry, J. L., Denneau, L., Heinze, A. N., et al. 2018, PASP, 130, 064505
- Torres, M. A. P., Casares, J., Jiménez-Ibarra, F., et al. 2020, ApJ, 893, L37
- Torres, M. A. P., Casares, J., Jiménez-Ibarra, F., et al. 2019, ApJ, 882, L21
- Wang, Y. D. & Bellm, E. C. 2023, The Astronomer's Telegram, 16209, 1
- Wood, C. M., Miller-Jones, J. C. A., Bahramian, A., et al. 2024, ApJ, 971, L9
- Wu, J., Jonker, P. G., Torres, M. A. P., et al. 2015, MNRAS, 448, 1900
- Yu, W., Bu, Q.-C., Zhang, S.-N., et al. 2024, MNRAS, 529, 4624
- Zhu, H. & Wang, W. 2024, ApJ, 968, 106
- Zurita, C., Casares, J., & Shahbaz, T. 2003, ApJ, 582, 369

Appendix A: Additional figure

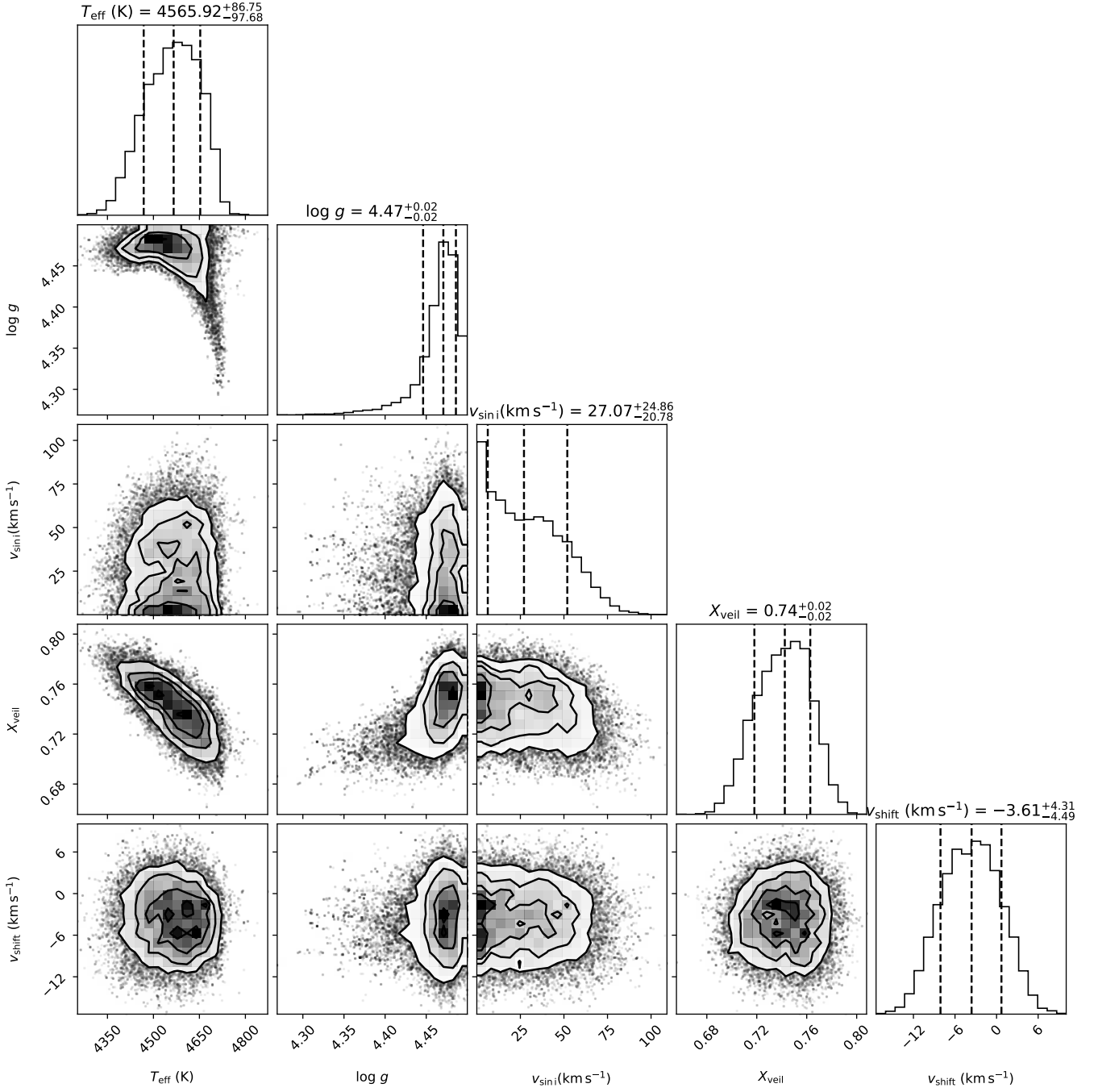


Fig. A.1. Corner plot for the free parameters of the EMCEE spectral classification. Contours in the 2D plots correspond to the 0.5 σ , 1 σ , 1.5 σ , and 2.5 σ levels (respectively containing 11.8, 39.3, 67.5, and 86.5 % of the volume), while in the marginalised 1D distributions the 0.16, 0.50, and 0.84 quantiles are marked with dashed lines.